Fundamentals of Electrical and Electromagnetic Techniques for CO_2 Monitoring

Erika Gasperikova[1] and H. Frank Morrison[2]

[1]Lawrence Berkeley National Laboratory, Energy Geosciences Division, Berkeley, USA

[2]University of California, Berkeley, USA

1. Introduction

Electrical and electromagnetic (EM) techniques are used to map the electrical resistivity of the Earth's interior. This resistivity is in turn dependent on key formation properties such as porosity, pore fluid resistivity, and fluid saturation. Electrical and EM techniques make use of the measurement of electric (E) and magnetic (B) fields caused by currents that are injected into the ground by contacting electrodes or induced to flow into the ground by inductive sources of a time-varying magnetic field. Current can be injected at the surface or in boreholes using a power supply driving a cable connected to metal electrodes embedded in the formation. Inductive sources are usually multi-turn coils of wire carrying an alternating current; they can have arbitrary orientation on the surface, but are usually confined to vertical solenoids if used in boreholes. Electric fields are obtained by measuring the voltage drop ΔV between two contacting electrodes separated by a distance dL. If dL is small the electric field is approximately $E \approx \frac{\Delta V}{dL}$. Electrical techniques, usually referred to as resistivity techniques, use only current and voltage measurements at frequencies low enough that there are negligible EM induction effects. EM techniques require frequency-dependent sources to induce currents in the ground and/or in conductive bodies in the ground. Magnetic fields are produced from currents created from both types of sources.

The basic concept in both techniques is to measure the electric and magnetic fields caused by the injected or induced currents, and to infer from these measurements the configuration and amplitudes of the current in the Earth and hence the distribution of electrical resistivity. There are two broadly defined areas of application. The first is the mapping of the resistivity in the subsurface; the second is to map the electrical properties, size, and shape of a localized region of interest. The first is used for broad geological mapping, such as determining depth to basement, structural mapping, aerial distribution of aquifers, etc., and it requires large aerial coverage combining information versus depth, called sounding, and horizontal location. The second application is more focused, because there's usually a conceptual geological model of a target zone, and the configuration of the sources and receivers, and the frequency of operation, can be optimized for the target. Carbon dioxide (CO_2) is usually injected into relatively flat lying formations and is expected to result in lenticular lenses or plumes of a finite size and of increased resistivity so the focus of this study will be on the response of flat lying localized resistive targets (Figure 1). Scenarios with complex interactions between CO_2, brine, and rock that result in anomalies that could be resistive or conductive require electrical monitoring governed by site-specific numerical simulations, and are beyond the scope of this chapter.

For localized features, there must be a contrast in resistivity with the enclosing formation; the goal of the survey is to identify a local variation in resistivity relative to the background geology. The perturbation of resistivity and the associated perturbation in the measured electric and magnetic fields are referred to as *anomalies*. Measurements of the anomalies in these fields over time are referred to as *monitoring*.

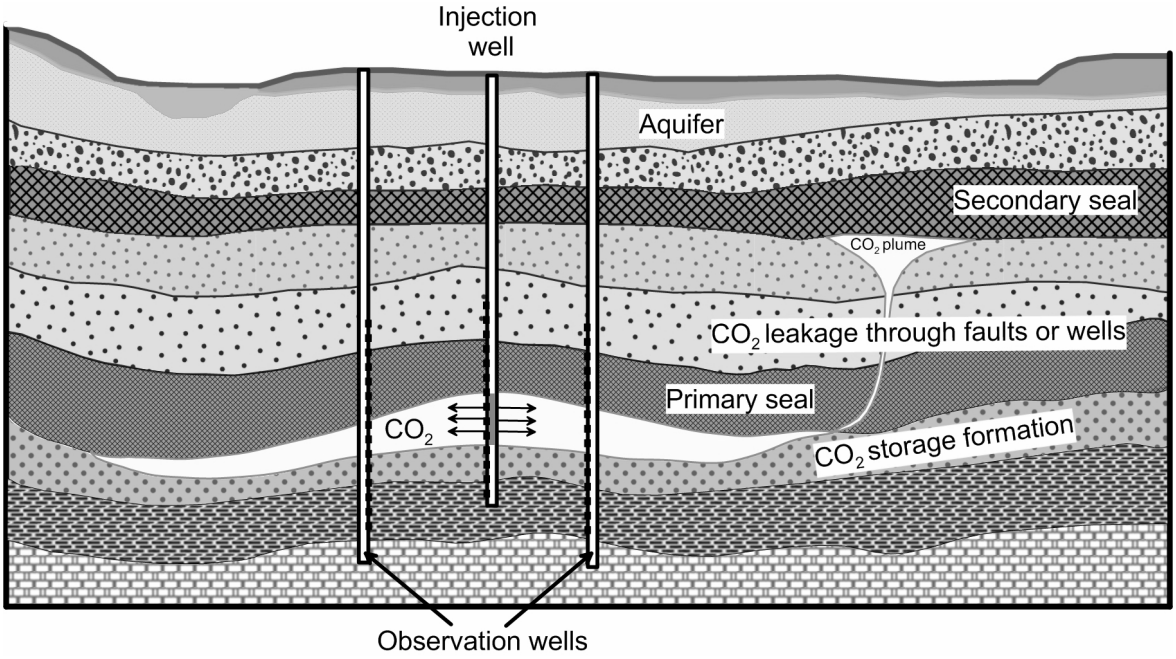

Figure 1. Schematic sketch of a typical geological setting for CO_2 injection and monitoring.

If the subsurface structure and its physical properties were precisely known, the field values could be predicted uniquely by forward modeling. In geophysical surveying, the problem is the opposite – namely, to infer the properties of the subsurface structure on the basis of measurements taken on the ground surface. This is known as an inverse problem. For practical reasons there cannot be sufficient sources and receivers deployed on the surface and throughout the subsurface to uniquely specify resistivity distribution. With limited sources and receivers on the surface and/or in boreholes the inverse problem suffers from an inherent ambiguity, or non-uniqueness. Many different subsurface structures could reproduce the observed measurements so interpretation depends on choosing a basic model of the subsurface based on other information (resistivity well logs, seismically derived structure, etc.) and then varying the parameters of that model to fit the data. Geophysical interpretation is therefore aimed at determining properties of the subsurface that all possible solutions share or introducing assumptions that limit the number

of admissible solutions [Parker, 1977]. The situation is somewhat improved in the study of localized target regions, especially for time-lapse monitoring. There is often a good conceptual geologic model of the target zone and the configuration of the sources and receivers, and the frequency of operation can be optimized to better resolve the properties of the target.

2. Physical properties of carbon dioxide (CO_2)

Carbon dioxide (CO_2) usually behaves as a gas in air at standard pressure and temperature or as a solid (called dry ice) when frozen. If the temperature and pressure are increased to or above the critical point (temperature of 31°C and pressure of 7.4 MPa), it behaves as a supercritical fluid (Figure 2). While the resistivity of CO_2 does not change whether it is in a supercritical or a gas phase, the phase does affect the volume that it fills. Under supercritical conditions, CO_2 has the properties of a gas, but behaves as a liquid, therefore CO_2 takes a much smaller volume than if it would be in a gas phase. This is very advantageous because more CO_2 could be stored under supercritical conditions than in the gas phase. These conditions appear at depths greater than 800 m. Because CO_2 is less dense than brine, it migrates upward, and a CO_2 plume tends to float above the brine, which translates to more resistive anomalies due to CO_2 over less resistive brine.

Brine-bearing formations that are below and hydrologically separated from potable water reservoirs have been widely recognized as having high potential for CO_2 sequestration. The following study is focused on the use of electrical and EM techniques for mapping the injection of resistive liquid CO_2 into reservoir-like formations at depth.

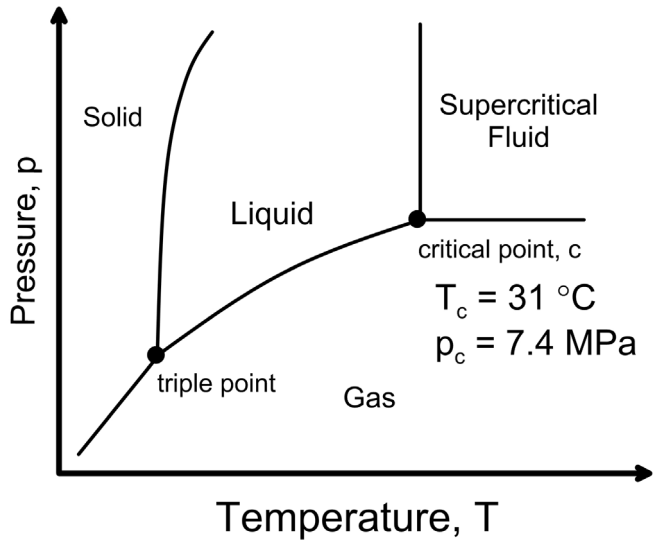

Figure 2. CO_2 phase diagram.

3. Rock properties and resistivity

The electrical resistivity of formation rocks is highly sensitive to changes in water saturation. This can be seen from Archie's Law [Archie, 1942], which is commonly used to describe the electrical resistivity (ρ_b) of sedimentary rocks as a function of water saturation (S_w), porosity (ϕ), and pore fluid resistivity (ρ_w).

$$\rho_b = a\,\phi^{-m}\,\frac{\rho_w}{S_w^n} \tag{3.1}$$

where a is tortuosity, and m and n are constants with $1.8 < m \leq 2$ and $n \cong 2$.

Fluid resistivity, ρ_w, depends on salinity (salt concentration) and temperature. Figure 3 illustrates this depencence using NaCl.

This empirical relationship was derived for clay-free sandstones, but subsequent works with other rocks and unconsolidated sediments shows that this power law is generally valid, though

with varying coefficients and exponents. Keller [1987] summarizes coefficients for different materials listed in Table 1.

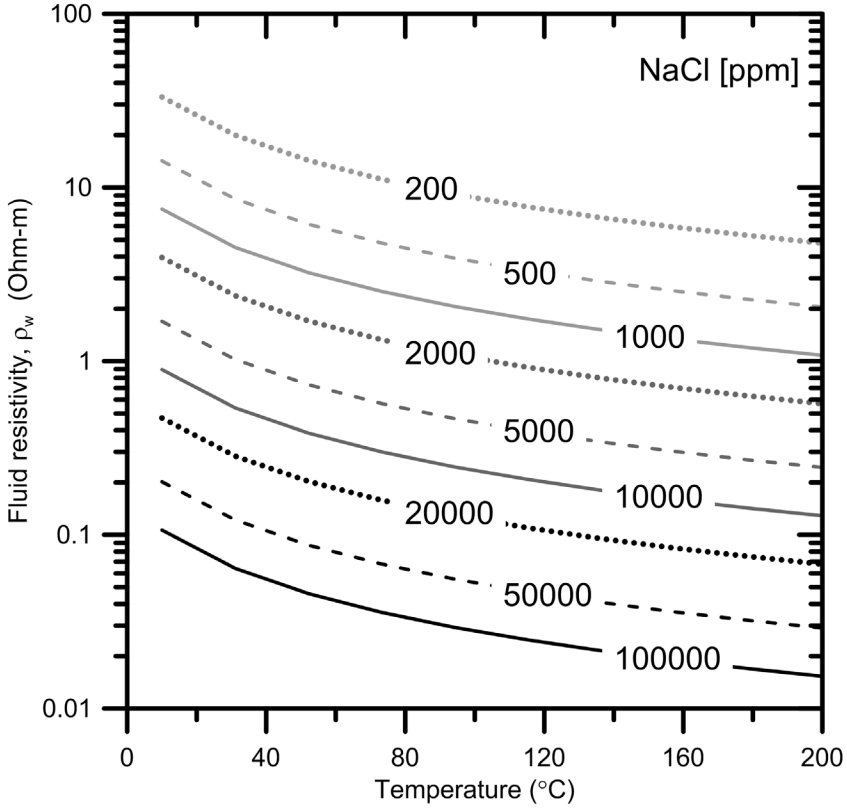

Figure 3. Fluid resistivity as a function of NaCl concentration and temperature.

Rock	ϕ	a	m
Weakly cemented, detrital (Tertiary)	0.25 – 0.45	0.88	1.37
Moderately well cemented (Mesozoic)	0.22 – 0.35	0.62	1.72
Well cemented (Paleozoic)	0.05 – 0.25	0.62	1.95
Dense, igneous, metamorphic	< 0.05	1.4	1.6
High porosity volcanic	0.2 – 0.8	3.5	1.4

Table 1. Values of porosity and Archie's coefficients a and m for various rock types [from Keller, 1987].

Because this relationship is not accurate in zones of moderate-to-high shale various ranges of *a*, *m*, and *n* coefficients and formulations have been proposed [e.g., Mabrouk et al., 2012; Kamel et al., 2002.] Kennedy and Herrick [2012] provide an excellent tutorial on the general applicability of Archie's law.

In a CO_2 sequestration scenario, CO_2 would be injected into a formation originally filled with brine, and therefore replacing brine with CO_2 results in CO_2 saturation $S_{CO2} = 1 - S_w$. Figure 4 shows the rock bulk resistivity (ρ_b) as a function of CO_2 saturation (S_{CO2}) for the formation with brine resistivity of 0.3 Ohm-m and 35% porosity. CO_2, as well as all petroleum fluids (oil, condensate, and hydrocarbon gas) are electrically resistive, hence the relation shown in Figure 4 is appropriate for any combination of oil, hydrocarbon gas, condensate, or CO_2.

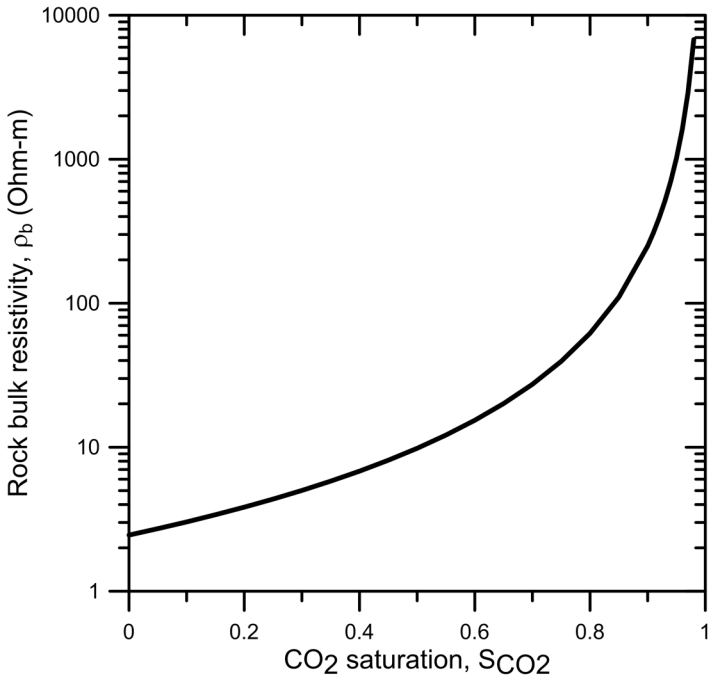

Figure 4. Rock bulk resistivity (ρ_b) as a function of CO_2 saturation (S_{CO2}). Pore fluid resistivity is 0.3 Ohm-m, porosity is 35%, a =1, m = 2, and n=2.

The rate of increasing temperature with depth is called a geothermal gradient, and it varies both with tectonic settings and with the thermal properties of the rock. High gradients are observed along the oceanic spreading centers or island arcs. Low gradients are observed in tectonic subduction zones. Tectonically stable shield areas or sedimentary basins have average gradients of 15-30°C per km of depth. Resistivity is inversely proportional to the temperature (e.g., a body of 30 Ohm-m at 100°C will have resistivity of 90 Ohm-m at 20°C). A similar relationship holds for resistivity and salinity; the higher the salinity, the lower the resistivity (e.g., TDS (total dissolved solids) of 1,000 ppm (parts per million; 1 ppm = 1 mg of salt in 1 liter of water) would have a resistivity of 90 Ohm-m, while TDS of 20,000 ppm would have a resistivity of only 5.5 Ohm-m). These numbers can be calculated using charts [Schlumberger, 1989] or a simple simulator (http://appliedgeophysics.berkeley.edu/dc/archie/index.html). Figure 3 shows this relationship for fluid resistivity.

Electrical resistivity can be measured by various electrical and EM techniques and then used to determine CO_2 saturation:

$$S_{CO_2} = 1\text{-}S_w = 1 - \frac{a\,\rho_w}{\varphi^m \rho_b}. \qquad (3.2)$$

In the presence of complex mineral composition, parameters used for Archie's equation may vary significantly, which may affect the selection of bulk rock parameters, and estimates of CO_2 saturations might not be accurate. In such an environment, one can use another useful and simple relationship between resistivity and brine saturation, the resistivity index [Archie, 1942; Gueguen, 1994]:

$$\mathrm{RI}=\frac{\rho}{\rho_0}=(S_w)^{-n}, \tag{3.3}$$

where ρ is resistivity of the rock partially saturated with brine, ρ_0 is the resistivity of fully saturated rock with brine, and n is the saturation exponent. The resistivity index is closely related to Archie's second law for partially saturated rocks with brine. Again, in the case of CO_2 injection, we can estimate CO_2 saturation from the initial resistivity of the fully saturated rock with brine and partial brine saturation during CO_2 injection using:

$$S_{CO_2}=1-\left(\frac{1}{RI}\right)^{1/n}. \tag{3.4}$$

When a formation contains a substantial amount of clay, an additional parameter – the ratio of volume of sand to volume of clay is necessary [e.g., Waxman and Smits, 1968; Nakatsuka et al., 2010].

4. Basic Principles of Electrical and Electromagnetic Techniques

4.1 Resistivity Techniques

Resistivity is a material property that describes the resistance to current flow when a voltage is applied across a sample of the material. Ohm observed that for most materials that conduct electric current there was a constant of proportionality R, the resistance in Ohms, between the current flowing through a sample of length L and cross section A and the applied voltage across the sample given by R = V/I.

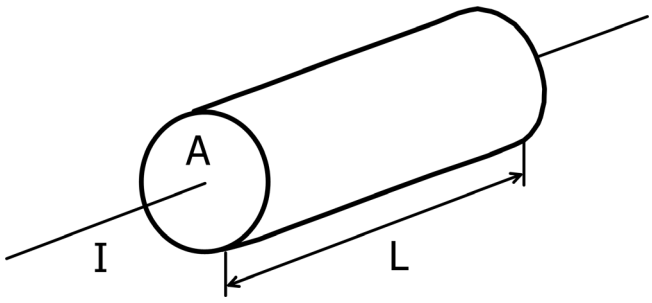

Expressed in terms of the electric field E = V/L in volts per meter (V/m) and current density J = I/A in amperes per square meter (A/m^2) this becomes the resistivity ρ (Ohm-m):

$$\rho = \frac{E}{J} = R\frac{A}{L} \tag{4.1}$$

The relation $J = \frac{E}{\rho}$ is Ohm's law and it defines the resistivity. It is often written as $J = \sigma E$, where $\sigma = \frac{1}{\rho}$ is the conductivity in siemens per meter (S/m). If the cross sectional area of the sample shown is 1.0 m^2 and the length is 1.0 m then $\rho = R$.

Many sedimentary sections and individual formations are banded, i.e., they are made up of many layers of differing resistivity and consequently the resistance is different for current flow transverse (or perpendicular) to the bedding from that along (or parallel) to the bedding. The simple model below is of a 1.0 m cube of resistivity ρ_1 with a single layer of fractional thickness *t* of resistivity ρ_2.

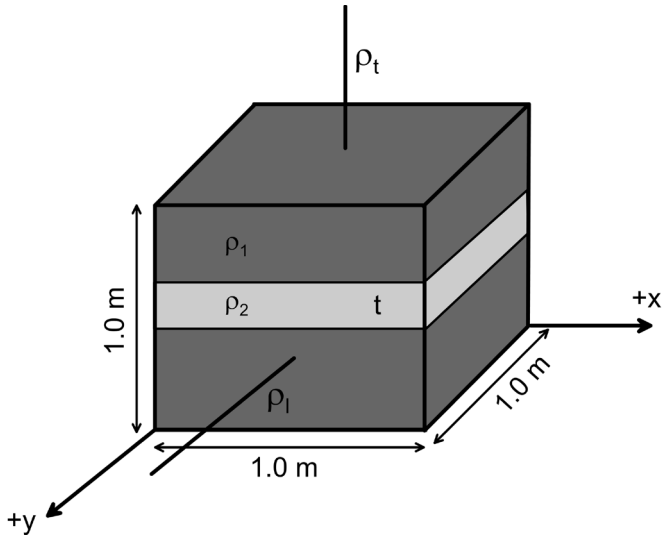

The transverse resistance for a 1.0 m cube is the *transverse resistivity* ρ_t and is the sum of the series resistance of the layer of thickness *t* and the remainder of the block of thickness *1-t*:

$$\rho_t = \rho_2 t + \rho_1(1-t) \tag{4.2}$$

If *t* is small and $\rho_2 < \rho_1$ then ρ_t is close to ρ_1. *Thin conductive beds have little effect on the transverse resistivity.*

The resistivity along the bedding, the *longitudinal resistivity* ρ_l, is given by the parallel resistance formula:

$$\frac{1}{\rho_l} = \frac{t}{\rho_2} + \frac{1-t}{\rho_1} \quad \text{or} \quad \rho_l = \frac{\rho_1 \rho_2}{t\rho_1 + (1-t)\rho_2} \tag{4.3}$$

If *t* is small and $\rho_2 \gg \rho_1$ then ρ_l is close to ρ_1. *Thin resistive beds have little effect on the longitudinal resistivity.*

From the basic definition of resistivity, and the fact that most surface-based electrical and electromagnetic methods involve the production of currents flowing parallel to bedding planes, it

can be anticipated that thin layers or lenses of high resistivity caused by CO_2 injection may be difficult to detect.

The resistivity of the ground is measured by a means analogous to that used for the sample described above. A current can flow in the ground if it is injected by means of a current source, a wire and two electrodes (A, B) (Figure 5), called an electric bipole.

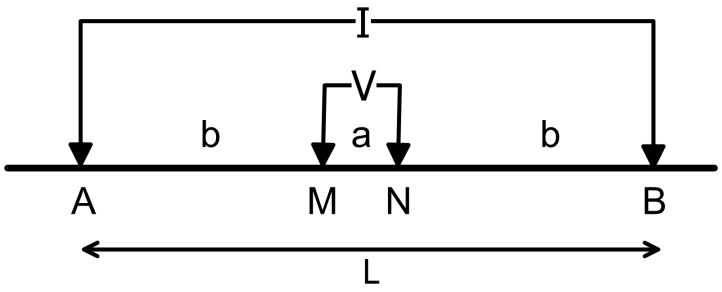

Figure 5. Example of an electrode array for a surface electrical survey. A and B are current electrodes, M and N are voltage electrodes, a is spacing between potential electrodes, b is spacing between current and potential electrodes, L is total array length, I is current, V is voltage.

Since current is conserved, the current in the ground is the same as the current in the wire (I), which is easily measured. The current in the ground produces two fields, an electric field, **E**, given by Ohm's Law:

$$\mathbf{J} = \sigma\, \mathbf{E} \qquad \text{(in siemens per meter, S/m)} \qquad (4.4)$$

of the ground, and a magnetic field (**B**) given by the Biot-Savart's Law:

$$\mathbf{B} = \frac{\mu_0}{4\pi}\int_V \frac{\mathbf{J}\times\mathbf{r_1}}{r^2}dV\,, \tag{4.5}$$

where $\mu_0 = 4\pi 10^{-7}$, dV is a volume element and r is the position where the magnetic field **B** is calculated.

The direction of the field follows the "right-hand rule" – with the thumb of the right hand in direction of current, then the fingers point in the direction of **B**. The Biot-Savart Law leads directly to a useful formula for the magnetic field from a short length of wire *dL* carrying a current **I** in a conductive medium (an electric dipole *p)*:

$$\mathbf{B} = \frac{\mu_0}{4\pi}\frac{\mathbf{I}\,dL\times\mathbf{r}}{r^2} \tag{4.6}$$

The electric field can be intuitively understood as the voltage drop per unit separation measured between two electrodes (M, N in Figure 5) by an ideal voltmeter in the medium (an ideal voltmeter drains no current and has itself no impact on current distributions). If a << b, V/a ~ E in volts per meter (V/m). For surface electrical surveys the necessary current and voltage electrodes are on the surface as shown in Figure 5, but they also can be in boreholes. If the ground is of uniform resistivity, the current (I) injected and the spacing of the electrodes (a, b) are known, then the measured voltage is linearly related to the ground resistivity through a simple formula. If the ground is not uniform, the currents will be distorted by the inhomogeneities and voltage measurements along the surface become indirect measures of the resistivity distribution. The array shown in Figure 5 is called the Schlumberger array. For sounding applications, from the surface, the distance b is varied, and as the spacing grows the

injected currents flow deeper into the earth, and the measured ΔV becomes sensitive to deeper layers or features. The value of ΔV in any resistivity survey is greatly influenced by the geometry of the source receiver configuration as well as by the resistivity distribution in the ground. To normalize the geometrical effect, the observed voltage for any source receiver array ΔV can be interpreted in terms of the resistivity of a uniform half-space that would give rise to the measured value of ΔV. This is called the apparent resistivity ρ_a and it is the standard means of portraying the results of resistivity surveys.

The injection of CO_2 is likely to form a lenticular or slab-like body and a resistive thin layer might be a good first-order model. A representative body is suggested in the sketch of Figure 1. A basic model for analyzing the detectability of such a body is a simple thin layer and a surface bipole source shown in the schematic drawing of Figure 6.

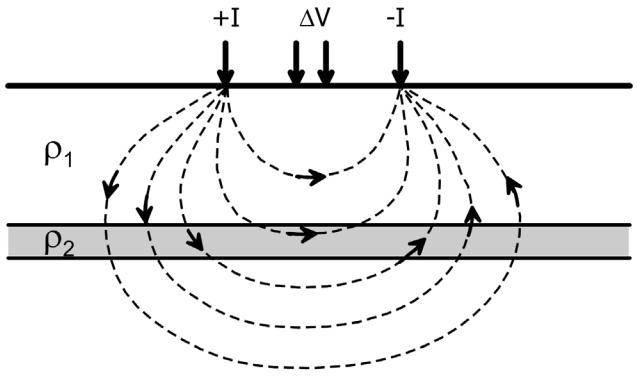

Figure 6. Surface bipole source and thin resistive layer model.

It might be expected from a consideration of the current flow lines that a thin resistor would block vertical current flow, with some shunting of horizontal current flow directly beneath the

bipole, but would have a major effect on the apparent resistivity. A thin conductor would have very little effect on the vertical currents and would not perturb the apparent resistivity appreciably. In fact, accurate numerical modeling of the Schlumberger response of resistive and conductive layers shows a comparable effect, as seen in Figure 7. Here, the background resistivity is 100 Ohm-m, with the layer resistivity either 10 or 1000 Ohm-m. Each layer causes ~13% response change.

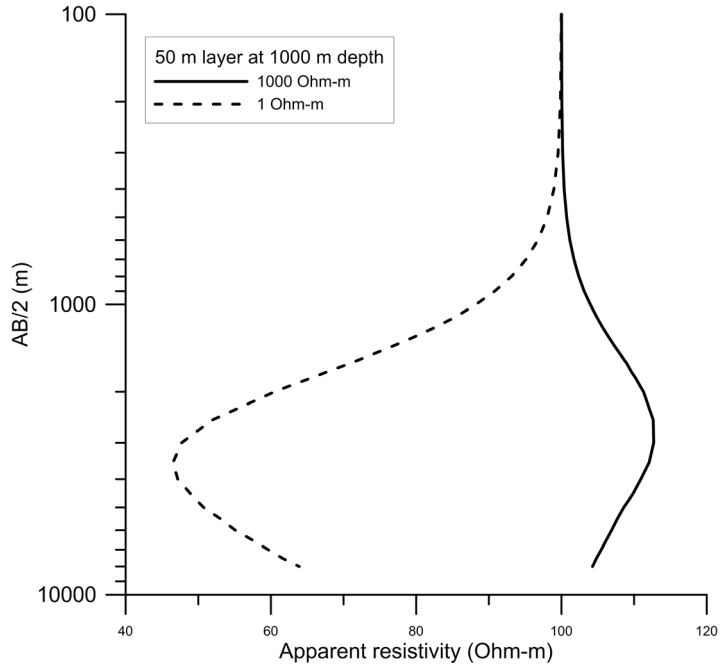

Figure 7. Schlumberger response of deep conductive and resistive layers.

A lower sensitivity to horizontal thin resistors is a manifestation of a fundamental property of the response of vertically anisotropic half-spaces. Keller [1966] showed that for an anisotropic half-space characterized by a vertical or transverse resistivity ρ_t and longitudinal or horizontal resistivity ρ_l (the coefficient of anisotropy is defined as $\lambda = \sqrt{\frac{\rho_t}{\rho_l}}$), the apparent resistivity for a

surface-based array is given by $\rho_a = \lambda \rho_l$ or $\sqrt{\rho_t \rho_l}$. On a macroscopic scale, an alternating sequence of equal thickness layers of 100 and 10 Ohm-m resistivity has a transverse resistivity of 55 Ohm-m and a longitudinal resistivity of 18.2 Ohm-m. The transverse resistivity is biased towards the resistive layer while the longitudinal resistivity is biased towards the low resistivity layer. Current flow from a surface electrode is impeded by resistive layers, but longitudinal flow in conductive layers reduces the blocking effect. For the alternating sequence above, the apparent resistivity for a surface array would be 31.6 Ohm-m., closer to the longitudinal resistivity than to the transverse. These results are even more counter-intuitive for vertical electrode arrays in a borehole, where *the measured apparent resistivity is the longitudinal resistivity.* The current flow is most strongly influenced by the conductive layers in the section. This phenomenon is referred to as the paradox of anisotropy. The important conclusion is that in a generally conductive section surface and borehole DC resistivity techniques are relatively insensitive to flat lying resistive CO_2 layers.

Electrodes can be configured in many different patterns (Table 2). Bipole-bipole is a general term that can be used for any electrode configuration where the distance between current electrodes (AB) is different from the distance between the potential electrodes (MN) and separated by an arbitrary distance (BM). When the source and receiver distances are equal (AB=MN=a) and they are separated by a multiple of a (n*a), the array is called dipole-dipole. When one of the source (or potential) electrodes is far away (approximation of infinity), the distance AB (or MN) is significantly larger than BM, the arrays are called pole-pole or pole-dipole. Two other arrays that have potential electrodes nested between the current electrodes are

Wenner, in which AB=3*MN, and Schlumberger, in which MN<<AB, arrays. The reader is referred to general geophysics textbooks [e.g., Telford et al., 1990] for details about these arrays; each array is sensitive to different types of structures, and has advantages and disadvantages. To achieve the best results in CO_2 reservoir or plume monitoring most of them need to be combined and selected based on forward modeling and analysis of a model that captures the complexity of the geology at the monitoring site. The same arrays can be deployed in boreholes, in which case the formula for apparent resistivity contains 4π instead of 2π.

Array type	**Apparent resistivity formula**	**Depth of investigation (after Barker [1989])**
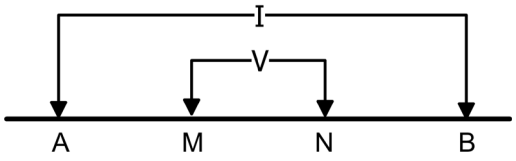 Wenner: AM=MN=BN=a	$\rho_a = 2\pi\ a\ \frac{V}{I}$	0.17*AB
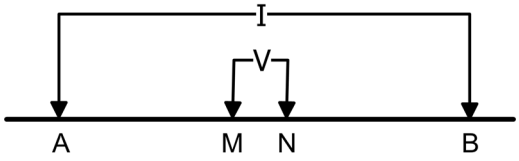 Schlumberger: MN=a, AM=BN=b, a<<b	$\rho_a = \frac{V}{I}\pi\frac{b\left(b+a\right)}{a} \approx \frac{V}{I}\pi\frac{b^2}{a}$	0.19*AB
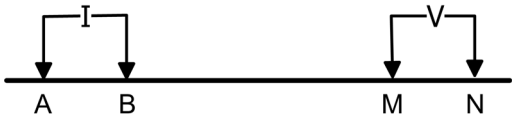 Dipole–dipole: AB=MN=a, BM=n*a	$\rho_a = \frac{V}{I}\pi\ a\ n\left(n+1\right)\left(n+2\right)$	0.25*AN
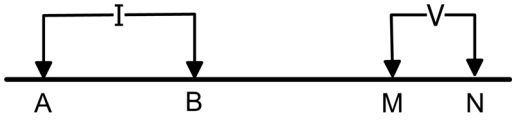 Bipole-bipole: $AB \neq MN \neq BM$	$\rho_a = 2\pi\frac{V}{I}\frac{1}{\frac{1}{AM}-\frac{1}{AN}-\frac{1}{BM}+\frac{1}{BN}}$	0.25*AN
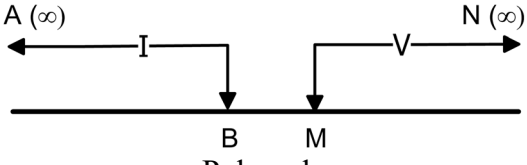 Pole-pole	$\rho_a = 2\pi\frac{V}{I}BM$	

Table 2. Electrode arrays

If the goal is to locate a deep body, an array is chosen in which both current and voltage electrodes are moved laterally and systematically along a profile or two-dimensional pattern on the surface. For the Schlumberger array, this would entail moving the center point of the array to successive points on the surface, and varying the b spacing at each position, which results in a combined lateral and depth profiling. To obtain the maximum information content with minimum operational difficulty it has been found that the dipole-dipole array is optimum.

An example to illustrate the response of a resistive body at depth is the model response of a cave in Figure 8. For this electrode array the current injection electrodes are widely separated and the measuring electric dipole is moved in increments between them (the Gradient array). The E-field is approximately uniform over the sphere. The cave is a perfect resistor and it distorts the current increasing the flow near the surface above it. This increases the voltage drop across the measuring voltage (potential) electrodes above the cave, which in turn produces an apparent increase in the apparent resistivity of the ground - the anomaly A. Physically and mathematically the inhomogeneity represents a secondary source that, in the case of the cave, creates a current pattern that opposes the incident current and reduces it to zero inside the body. For the spherical shape used in the example the opposing current field is that of a short length of current – a short wire with current flowing into the half-space from each end. That is the definition of an electric dipole.

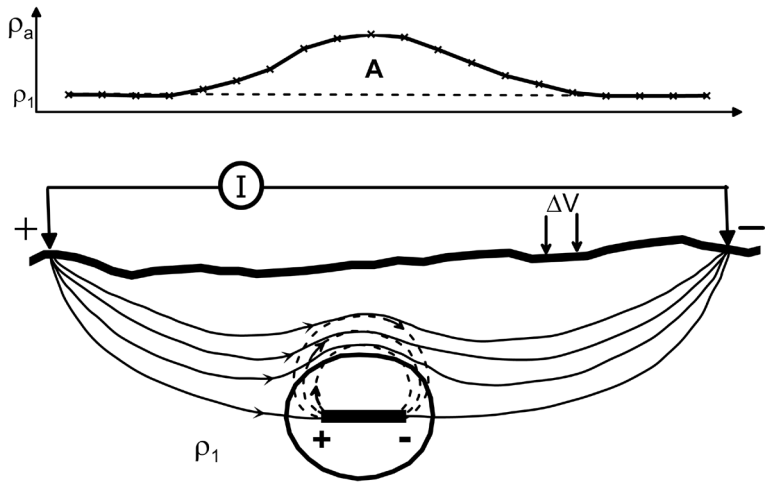

Figure 8. Example of an anomaly created by a spherical cave of infinite resistivity

The DC resistivity method is formally the low frequency limit of the general EM method, where the time rate of change of any magnetic fields is so small that Faraday induction can be ignored. At higher frequencies, the supply wires for the contacting electrodes also create time varying magnetic fields and so the currents in the ground have a component created by Faraday induction from the source. The magnetic field associated with the current flow consists of two components – (1) a field caused by the current in the wire connecting the electrodes, and (2) a component caused by the currents in the ground. Purely inductive sources, such as loops of wire carrying alternating current, need not contact the ground nor will they induce any current at zero frequency (DC). Time varying currents in the ground have their associated magnetic fields that interact with the source field modifying the entire induction process. At DC, if the ground is uniformly layered, the resulting magnetic field measured on the surface is independent of the ground resistivity and depends only on the magnitude of the current, the geometry of the source current lines and the location of the magnetic field detector. If the ground is inhomogeneous, the

current departs from the uniform distribution and the magnetic field measured on the surface depends on the resistivity distribution. Measuring the surface magnetic fields caused by subsurface resistivity inhomogeneities is the basis of the magnetometric resistivity method (MMR) [Edwards and Nabighian, 1991].

4.2 Electrical Resistance Tomography (ERT)

Electrical resistance tomography (ERT) is an indirect method for visualizing the movement of fluids in porous media requiring the intermediate application of inversion algorithms that convert raw measurements of electrical resistance to a tomographic image (resistivity or concentration) of a fluid plume. Spatial resolution, critical for ERT, is a complex function of numerous factors (e.g., electrode layout, measurement schedule, data quality, imaging algorithm, resistivity distribution). Figure 1 shows a typical geological setting for CO_2 injection and monitoring. A simplified model representing a CO_2 plume at a depth of 900 m and borehole ERT results of the plume are shown in Figure 9. The resistive body causes changes in apparent resistivity up to 60%; however, a contour of 50% change most closely resembles the outline of an anomalous region. ERT resistivities can also be used to determine CO_2 saturations using the rock properties models described in Section 3.

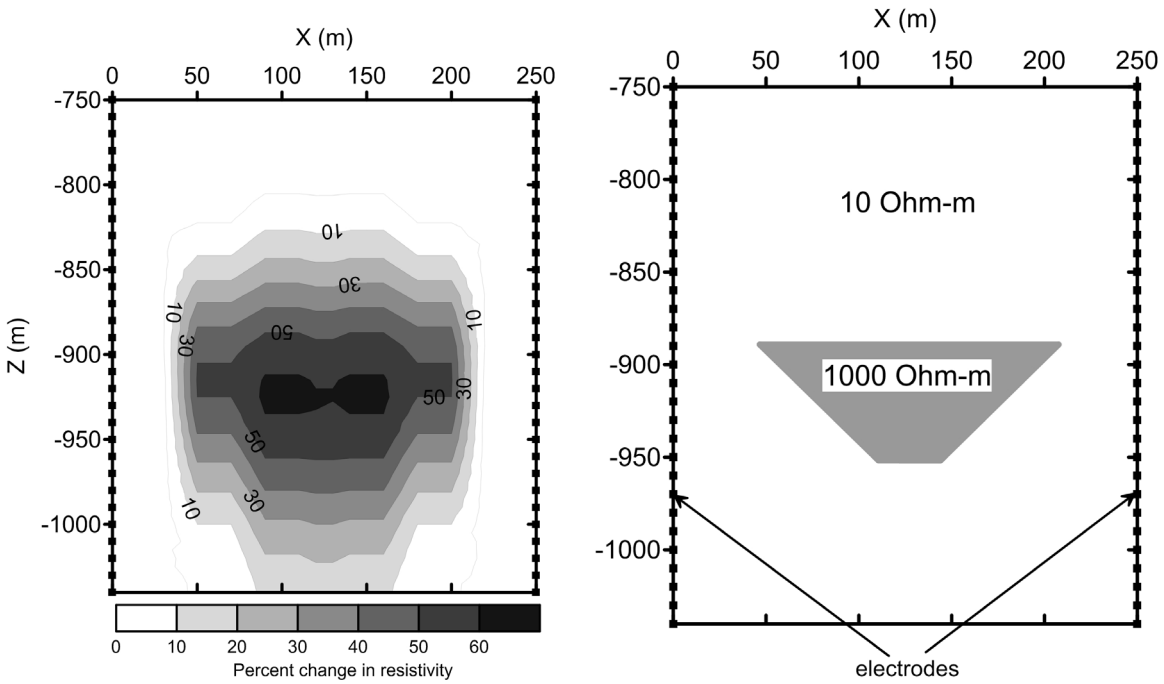

(a) (b)

Figure 9. (a) Change in electrical resistivity due to (b) CO_2 plume recovered by ERT.

Uncertainty in ERT tomographic images and ERT-derived CO_2 saturation may come from many sources, such as data noise, electrode location errors, regularization parameters, numerical and model errors, assumptions in Archie's equation, and choice of inversion constraints. For borehole arrays, electrodes need to be permanently installed in the boreholes within a depth interval at least as great as the distance between boreholes. The image resolution also depends on the distance between boreholes. Electrode configuration would be based on forward modeling and analysis of models that capture complexity of the geology at the monitoring site. The advantage of crosshole ERT is that the CO_2 injection or the reservoir can be monitored in detail because of measurements proximity to the source or target of interest. The disadvantage of this array is its very limited areal coverage, and thus it is not suitable for monitoring leakage over large areas from underground storage zones. For this purpose, borehole-to-surface or surface

measurements are more appropriate.

4.3 Electromagnetic (EM) techniques

The current loops carrying an alternating current or grounded current sources injecting alternating current have an associated changing magnetic field, which through Faraday's law induces currents to flow in the ground or in inhomogeneities within the ground. Faraday observed that a time varying magnetic field passing through a circuit produced an electromotive force, emf, that was proportional to the time rate of change of the magnetic flux threading the circuit. The total flux, $\mathbf{\Phi}$, through the circuit is defined as the integral of the component of $\mathbf{B}$ normal to the surface contained by the circuit:

$$\mathbf{\Phi} = \int \mathbf{B} \cdot \mathbf{ds} \tag{4.7}$$

Faraday's Law then states that an emf is produced in the circuit according to:

$$\text{emf} = -\frac{d}{dt}\int \mathbf{B} \cdot \mathbf{ds} = -\frac{d\mathbf{\Phi}}{dt} \tag{4.8}$$

In the circuit, the emf is the integral of the electric field around the circuit:

$$\text{emf} = \oint \mathbf{E} \cdot \mathbf{dl} = -\frac{d\mathbf{\Phi}}{dt} \tag{4.9}$$

Using Stokes' Theorem we find the differential form of Faraday's Law:

$$\nabla \times \mathbf{E} = -\frac{d\mathbf{B}}{dt}. \tag{4.10}$$

Taking the curl of both sides of Biot and Savart's Law, Equation (4.5) yields:

$$\nabla \times \mathbf{B} = \mu \mathbf{J} \tag{4.11}$$

which is known as the differential form of Ampere's Law.

With Ampere's Law, and Faraday's Law, and the constitutive relations, $\mathbf{J} = \sigma \mathbf{E}$, $\mathbf{B} = \mu \mathbf{H}$, and the fact that $\nabla \cdot \mathbf{B} = 0$, we have all the equations needed to solve any problem in low frequency electromagnetic induction.

Both the current source and receivers are usually multi-turn loops of wire. The field produced from a small multi-turn loop is proportional to its dipole moment, M, which is equal to the product of the current, I, the area of the loop, A, and the number of turns, N. The moment is a vector whose direction is normal to the plane of the loop (along the axis of the loop). The currents induced in the ground or in an object in the ground are a function of the time rate of change of the primary field at the object and of its size, shape, resistivity (ρ) and magnetic permeability (μ), and the resistivity and permeability of the surrounding medium. The response of the ground or a particular object is defined as the measured field for a given configuration of transmitter and receiver.

For most surveys to date for delineating subsurface layering or inhomogeneities sources are either horizontal or vertical loops of time varying current or electric bipoles or dipoles with time varying currents. Solutions for the fields from these sources on the surface of a layered half-space are summarized by Ward and Hohman [1987] and many others referenced there. *A major finding of these studies is that the electromagnetically induced currents in the layered half-space only flow horizontally: no induced vertical currents flow.* The implication for this study is that

surface based EM methods have the same limitations as surface DC electrical methods for detecting or delineating flat lying resistive features. Limited modeling using inductive sources has shown that the maximum anomalies from resistive targets are in fact obtained with electric dipole sources, and the lower the frequency the better. Increasing the frequency decreases the fields at the target through the skin depth effect, with a concomitant decrease in the secondary fields back on the surface from the induced dipole moments. For monitoring changes in a resistive body at depth there is no advantage in using EM effects; in fact, every effort should be used in surface electric dipole/bipole surveys to keep the frequency of operation low enough to minimize EM response.

Distributed magnetohydrodynamic current systems in the ionosphere and magnetosphere are another source of induced currents in the ground. These natural EM fields form the basis of the magnetotelluric (MT) technique [Vozoff, 1991]. These sources produce fields at the surface that behave as normally incident plane waves that reflect at the surface, but produce a field of orthogonal E and B components that diffuses into the earth with an exponential decay determined by the resistivity and frequency. The decay rate is the 'skin depth' δ given approximately by:

$$\delta = 500\sqrt{\frac{\rho}{f}} \quad [m] \tag{4.12}$$

where ρ is the resistivity and f is the frequency. The ratio of orthogonal E to B on the surface depends on the resistivity and frequency through a simple expression that can be rearranged to

yield an expression for the apparent resistivity of the ground - $\rho = \frac{0.2}{f}\left|\frac{\mathbf{E}}{\mathbf{B}}\right|^2$ when **E** is in microvolts per meter and **B** is in nanoTesla. In a sounding of a layered model, the basic idea is that high frequencies (small skin depths) yield apparent resistivities for the uppermost layer, and as the frequencies decrease the apparent resistivities change reflecting the change in layer resistivity with depth.

5. Models for simple resistive bodies

5.1 Layer models

Since it is expected that injected CO_2 will likely spread out in a relatively flat lying lens or layer as suggested by Figure 1, the simplest first-order model to use for detectability analyses is a thin resistive layer. This model can be used to determine the maximum depth at which a resistive layer could be detected, and the maximum depth at which time changes in the layer could be monitored. Figure 10a shows the Schlumberger apparent resistivity response for a layer 50 m thick and resistivity of 1000 Ohm-m in a 100 Ohm-m half-space as a function of layer depth. The response curves show that the peak response of the layer shifts to increasing current electrode spacings as the layer becomes deeper. This immediately shows a practical deployment problem with the technique; the current electrode spacing has to be greater than 8 km (AB/2 = 4 km) to define the response curve for the layer at 1.0 km depth. Apart from the difficulty of laying current carrying cable on a path over 8 km long, it is unrealistic to assume that the local near surface geology would not have variations on such a scale whose resistivity inhomogeneities would distort the sounding response. If these near surface effects are constant in time, then it is

clear that from a monitoring point of view the layer anomalies are large enough to see changes in layer properties to great depths. Figure 10b shows that the anomaly from a layer at 1.0 km is almost 15%, and at 2 km it is still a relatively large 7% (albeit at an AB/2 of 6 km).

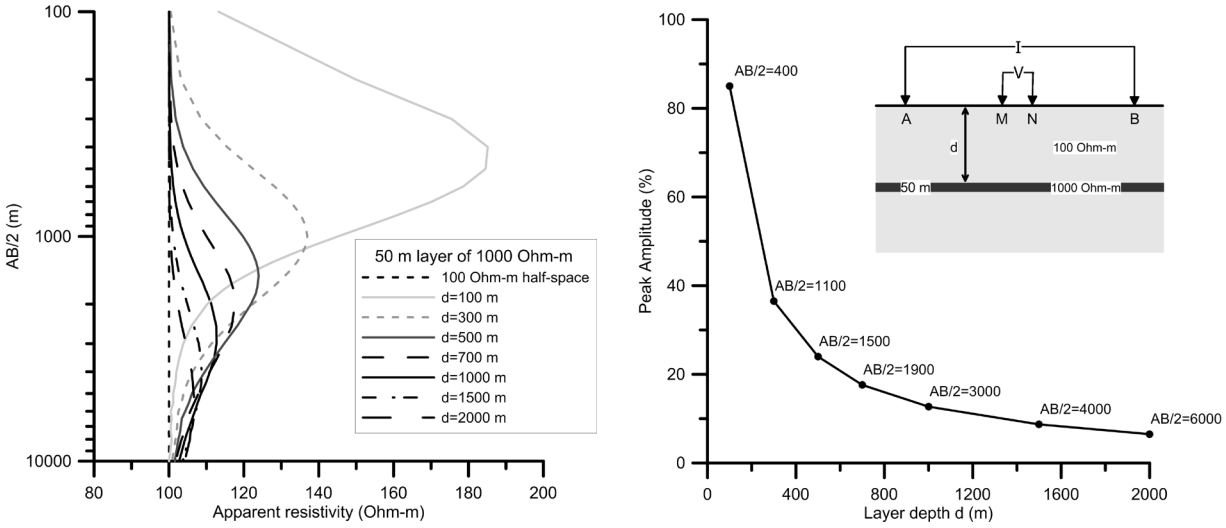

Figure 10. (a) Schlumberger apparent resistivity response for a layer 50 m thick and resistivity of 1000 Ohm-m in a 100 Ohm-m half-space as a function of layer depth. (b) Peak anomaly as a function of layer depth.

The response for a thin resistive slab of finite lateral extent is significantly less (Figure 11). This is a two-dimensional model, infinite in the y-direction. The slab is 50 m thick, 400 m in lateral extent, at a depth of 1.0 km. The response in Figure 11 is for a traversing dipole-dipole array. The dipole-dipole array combines sounding and lateral resolution, and has a significant deployment advantage in that cable needs only be laid between relatively closely spaced electrodes – depth of detection is achieved by increasing the dipole separation. Each dipole is 200 m long and the separation is kept at 2 km as the array moves in 200 m increments over the body. The apparent resistivities are plotted at the midpoint of the array for a conductive body and a resistive body. The saturation, a maximum response, occurs for $\rho_2 \geq 10\rho_1$ for the resistive

body, but only for $\rho_2 \le 0.03\rho_1$ for the conductive body. The conductive slab brings the apparent resistivity down by 7%, but the resistive slab increases it only by 1.6%. The resistive finite lense of CO_2 would be very difficult to detect or to monitor.

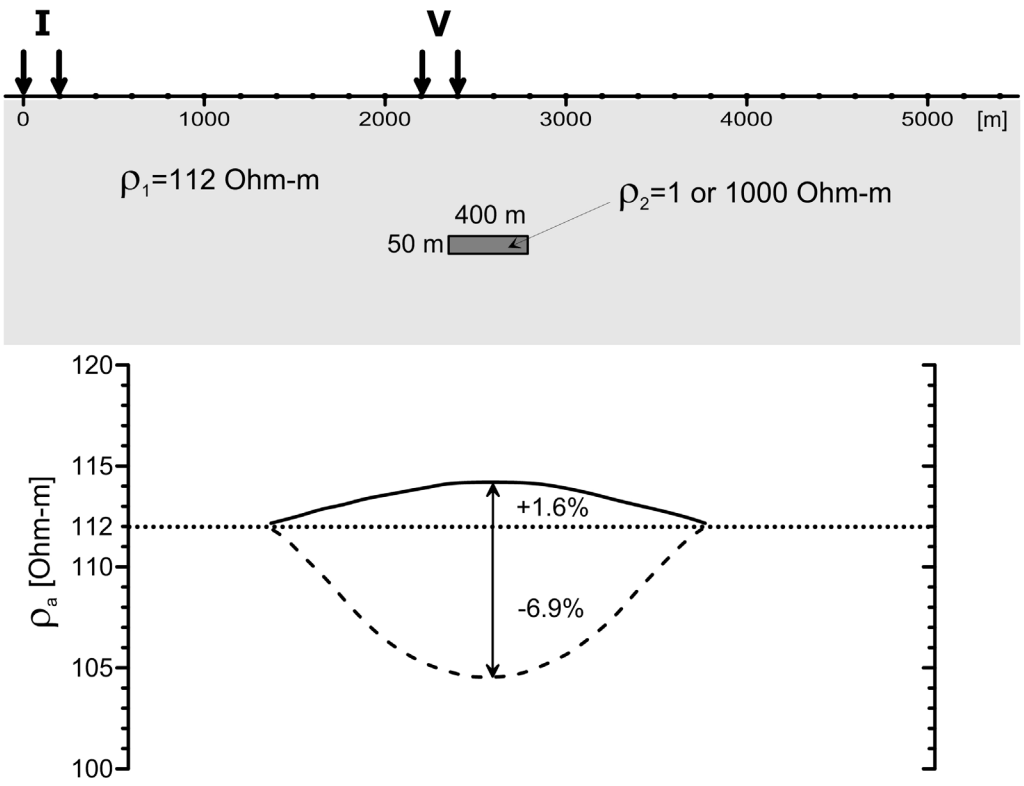

Figure 11. Dipole-dipole response for deep conductive and resistive bodies.

The sensitivity to thin finite-width horizontal resistors is even worse for natural magnetotelluric (MT) fields where the incident fields in a half-space are truly horizontal. The MT response for a model similar to that used for the dipole-dipole resistivity response, but with a thicker body, is shown in Figure 12. The apparent resistivity for two polarizations of the incident MT field, E perpendicular to strike (the TM mode) and E parallel to strike (the TM mode) are shown for both a conductive slab (ρ_2) and a resistive slab (ρ_3). There is a maximum TM response of only 3%

for the resistive body, but a response of ~43% for the TE mode over the conductive slab. The infinite resistive layer for these model parameters has a maximum anomaly of 5%. Interestingly, the slab response is only 40% less than the layer response, but in either case the layer or slab would be difficult to detect. Accounting for the increased thickness of the slab in this model, the response is still significantly less than the Schlumberger response for the layer at 900 m, ~16%. Here the incident fields are horizontal and the obstruction of a thin resistor causes almost no perturbation of the current and consequently of the response.

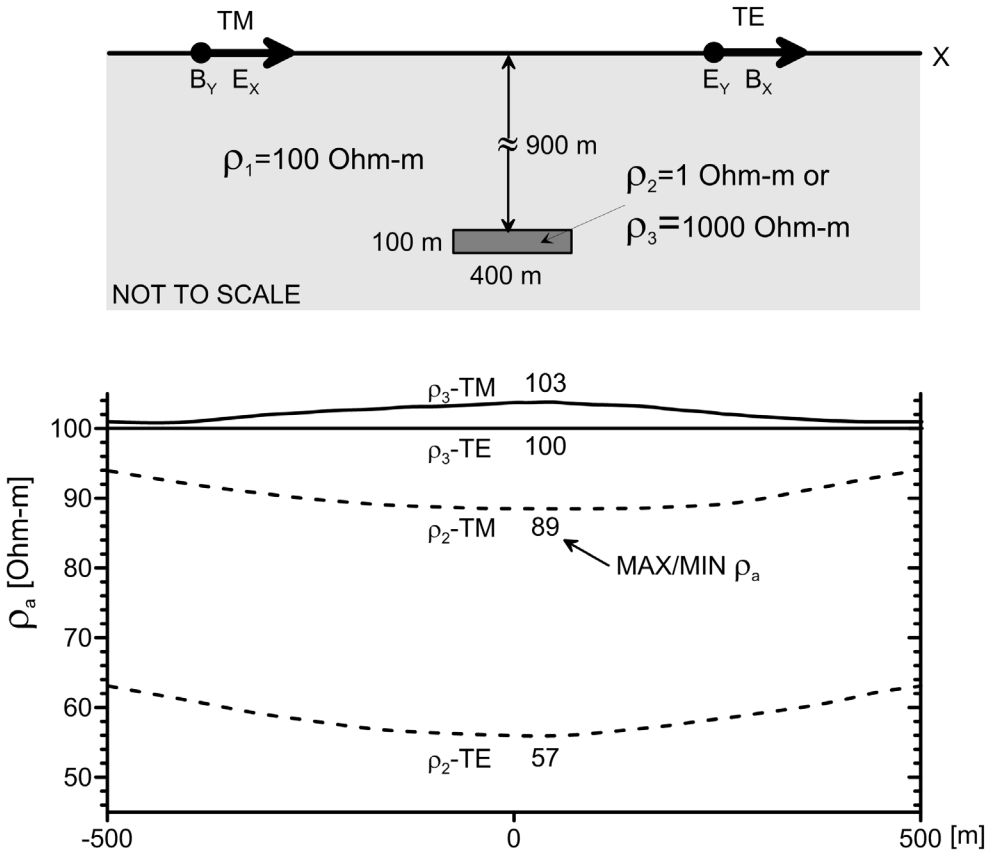

Figure 12. MT response for deep conductive and resistive bodies.

Finally, the surface EM response for a 100 m thick 1000 Ohm-m layer at a depth of 1.0 km for either a vertical magnetic dipole (horizontal loop) or horizontal magnetic dipole (vertical loop) on the surface is not distinguishable from the 100 Ohm-m half-space response for any practical transmitter-receiver separation and frequency. The response is even less than that for MT because the inducing fields at the layer fall off geometrically as $1/r^3$, in addition to the EM attenuation. It does not appear practical to use surface inductive sources for detecting or monitoring thin resistive layers at depth. This model result confirms the theoretical results that inductively induced currents flow only parallel to layer boundaries and are insensitive to resistive layers.

5.2 Sphere models

The sphere is a useful model for quantitatively studying the basic properties of the secondary fields produced on the surface by a finite body at variable depth and in a variety of source fields, and for obtaining estimates of the practical magnitude of the source currents needed. While it is unlikely that a volume filled with CO_2 would be spherical, it would be roughly confined within a formation (e.g., wedge, trapezoid), and order-of-magnitude rules for depth and size determination can be estimated using the sphere in Figure 13.

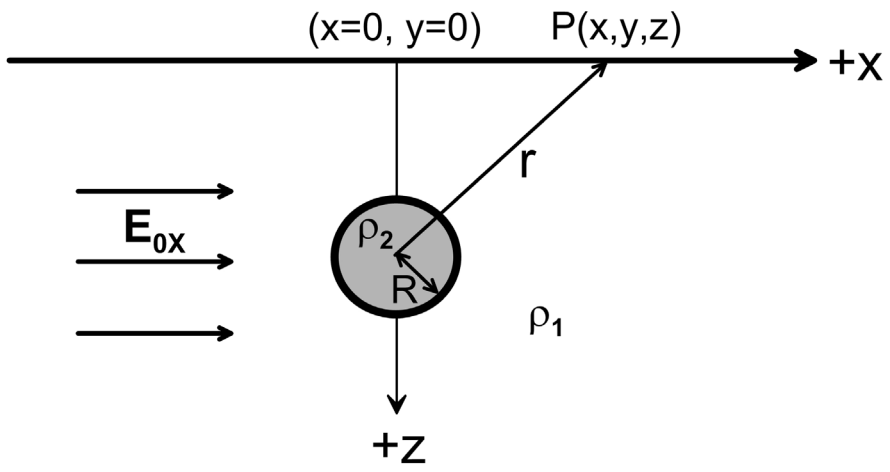

Figure 13. Spherical body in a uniform inducing field. P is the observation point, R is sphere radius, r is the distance, ρ_1 and ρ_2 are whole space and sphere resistivities, E_{0X} is inducing field.

The expression for the secondary or anomalous potential at an observation point P arising from a spherical body of resistivity ρ_2 and radius R in a whole space of resistivity ρ_1 and in a uniform inducing field E_{0x} is given by Ward (1967):

$$\phi^a = \frac{\rho_1 - \rho_2}{\rho_1 + 2\rho_2} E_{0X} R^3 \frac{1}{r^2} \cos\theta \tag{5.1}$$

but the potential of a simple current dipole of moment $p = I\,dL$ in a medium of resistivity ρ_1 is $\frac{p\,\rho_1}{4\pi}\frac{\cos\theta}{r^2}$, so the solution for a finite radius sphere is just that of a dipole of moment p, given by:

$$p = I\,dL = \frac{\rho_1 - \rho_2}{\rho_1 + 2\rho_2} \frac{E_{0X} 4\pi R^3}{\rho_1} \tag{5.2}$$

This is a quantitative statement of the non-uniqueness problem: the external field only depends on the product of the size term and the resistivity contrast term. The expression also shows the saturation effect; the moment reaches a limit of $\frac{E_{0X} 4\pi R^3}{\rho_1}$ when $\rho_2 << \rho_1$, and half that and of the opposite sign, i.e., $-\frac{E_{0X} 4\pi R^3}{2\rho_1}$ when $\rho_2 >> \rho_1$. This phenomenon is characteristic of the anomalies of all finite bodies; the anomaly reaches an asymptotic value by the time the contrast exceeds 30 or so. Generally, the horizontal component of the electric field E_X is measured on a line over the sphere, so taking the x component of the negative gradient of the potential yields the following expression for E_X on a profile, a distance z above the sphere:

$$E_X = \frac{\rho_1 - \rho_2}{\rho_1 + 2\rho_2} E_{0X} R^3 \left[\frac{2x^2 - y^2 - z^2}{r^5} \right] \tag{5.3}$$

The maximum secondary field anomaly occurs directly above the sphere at x=0, y=0, and at –z, so the peak anomaly is:

$$E_X = \frac{\rho_1 - \rho_2}{\rho_1 + 2\rho_2} \frac{E_{0X} R^3}{z^3} \tag{5.4}$$

The above expressions were derived for a sphere in a conducting whole space. If the sphere was in a half-space whose surface was defined by the solid profile line in Figure 13, an approximate solution for the horizontal electric fields on the surface can be obtained by superimposing the solution for a second sphere an equal distance above the surface: this approximately doubles the surface fields. For this study, the target sphere is resistive and with the above approximation and assuming a very high contrast the anomaly becomes:

$$E_X = E_{0X}\left(\frac{R}{z}\right)^3 . \tag{5.5}$$

For a given sphere radius, the anomaly falls off as the inverse cube of the depth. The anomaly must be measured in the presence of the primary field, so there will be some measuring instrument limitation on the smallest ratio of E_X/E_{0X} that can be resolved. More important is the fact that the background half-space is generally not uniform nor is the ground surface a flat plane. The surface electric field will be highly variable due to near surface resistivity inhomogeneities and topography, and this background 'geologic noise' will determine the limit for detecting the sphere. This can be seen in the cartoon of Figure 14.

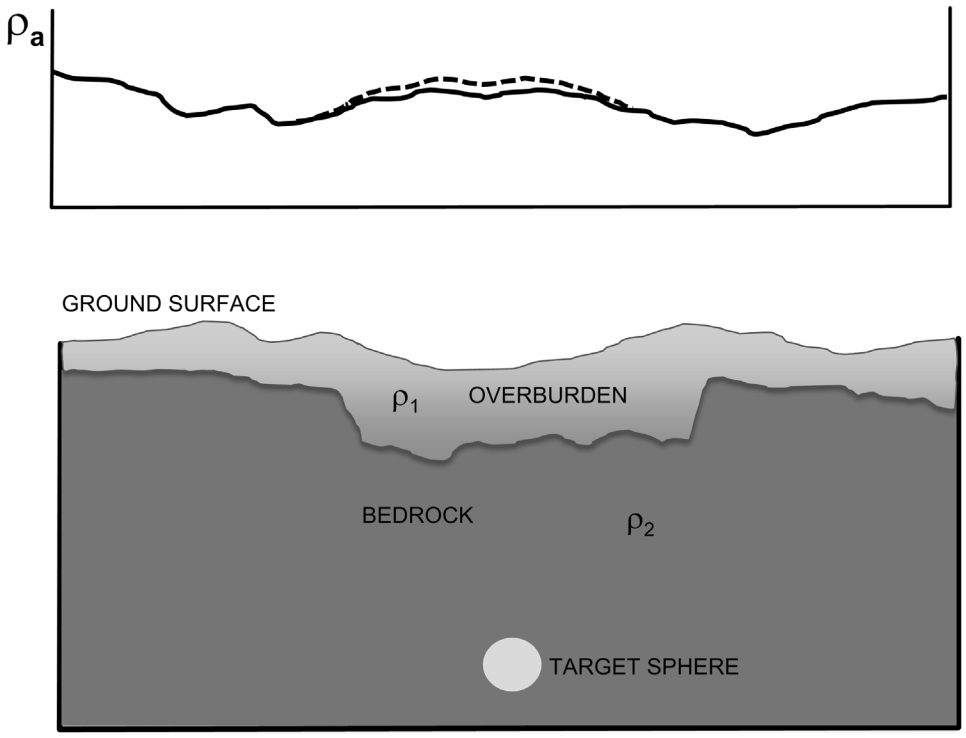

Figure 14. Geologic section with an irregular surface and overburden and sphere response.

A typical shallow geologic section has an irregular surface on a variable thickness overburden on an underlying bedrock formation. The surface electric fields, converted to apparent resistivity, ρ_a, are irregular and their perturbation by a target sphere at depth, shown by the dashed line profile in Figure 14, is very small. From a mapping point of view it is unlikely that changes in ρ_a or E_X/E_{0X} of less than 1.0 % could be identified as a target. This implies that R/z would have to be greater than $\sqrt[3]{10^{-2}}$ or ~0.22 to be detected. For a 50 m sphere the depth of detection would be limited to ~230 m. Somewhat counter intuitively a perfectly conducting sphere of the same radius could be detected to ~290 m. This simple model illustrates the fundamental limitation of any resistivity method for detecting resistivity anomalies at depths much greater than three times their dimension. However, for monitoring changes in the size of such a target over time, the full sensitivity of the measurements can be used, since the background surface electric field can be assumed constant, and so differences highlight the anomaly. The derivation above assumes that the incident electric field is constant with depth and uniform across the sphere. In fact, the field from any finite current source would decrease with depth so that the induced dipole moment in the sphere would also decrease with depth and so the anomaly would fall off faster than $1/r^3$. Further, since the size of the anomaly depends on the amplitude of the inducing field at the sphere, a more complete analysis for a representative source must be made to determine the currents that would be necessary to probe to a desired depth. To this end the horizontal field at the midpoint of the bipole of Figure 15, given a length L, versus depth is calculated via Telford et al. [1990]:

$$E_{0X}(z) = \frac{I\rho_1}{2\pi} \frac{L}{\left(z^2 + \frac{L^2}{4}\right)^{3/2}}. \tag{5.6}$$

At depths greater than the diameter of the sphere and for values of L greater than the depth of the sphere it can be assumed that this incident field is uniform across the sphere and this value of E_{0X} can be substituted in Equation (5.5) to find the anomalous E_X back at the surface. It is clear from Equation (5.6) that for a constant current the field decreases with increasing L and increasing z. Furthermore, when L << z the field falls off as $1/z^3$ and so the anomalous field falls off as $1/z^6$. For L >> z the field falls off as $1/L^2$ and then the anomalous field falls as $1/z^3$ as it would in a uniform field. These effects are most easily seen graphically in Figure 15, a plot of the anomalous horizontal field at the surface for a resistive sphere of 50 m radius versus depth of burial for a range of bipole lengths L, and $I\rho_1 = 1.0$.

In field surveys, the sensitivity limit is set by the noise level of the voltage measuring electrodes. For carefully installed metal-electrolyte electrodes and for capacitive electrodes this noise level is about $10^{-7} V/\sqrt{Hz}$ at 1.0 Hz. For a 100 m receiving dipole the field noise level would thus be $10^{-10} V/m/\sqrt{Hz}$. To resolve an anomaly its amplitude should probably be ten-times the noise so a detectable anomaly must have an amplitude of $10^{-9} V/m/\sqrt{Hz}$. Field transmitters can deliver 100 A into contacting metal sheet electrodes, and using 10 Ohm-m for a representative half-space gives $I\rho_1 = 1000$. Referring to Figure 15 the detection threshold is at 10^{-12} V/m and the maximum depth of detection is ~1.5 km with a 3 km transmitting bipole. Doubling the radius of the sphere to 100 m increases the maximum depth of detection to 2.5 km.

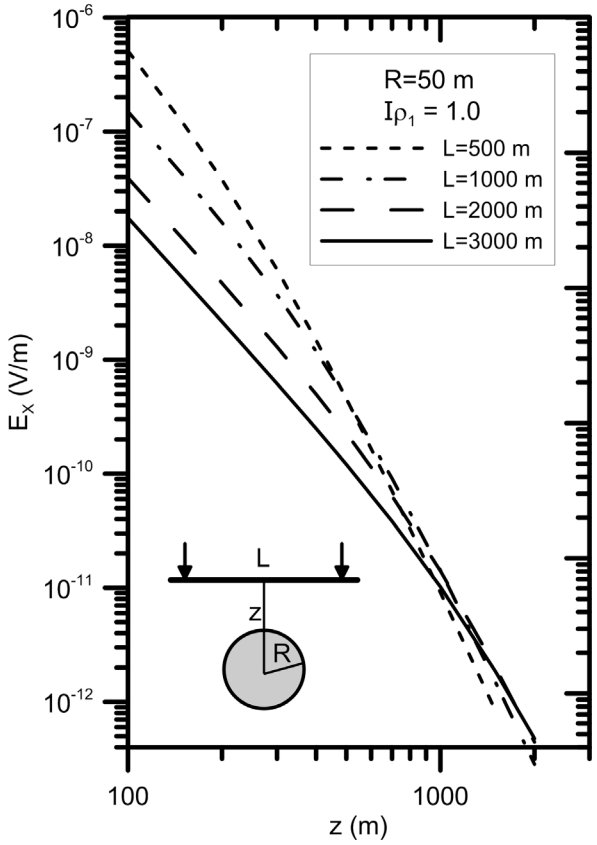

Figure 15. Anomalous horizontal field at the surface for a resistive sphere of 50 m radius as a function of depth and bipole length L and $I\rho_1 = 1.0$.

In practice, the surface anomalous field must be measured in the presence of the primary field – the field on the surface from the current electrodes emplaced on the background half-space $E_X^{Z=0}$. With a 20-bit voltage receiver the minimum resolvable signal would then be $\sim 10^{-6} \times E_X^{Z=0}$. A useful measurement signal should probably be ten-times this value. A plot of the anomalous signal from the 50 m test sphere normalized by the primary field is presented in Figure 16 as a function of the depth of the sphere for a variety of bipole lengths L.

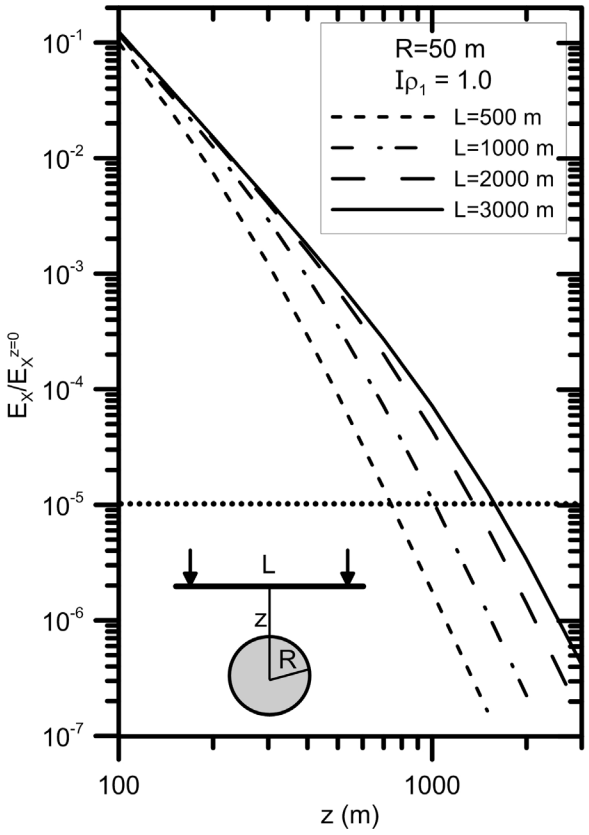

Figure 16. Anomalous signal normalized by the primary field for a resistive sphere of 50 m radius as a function of depth and bipole length L.

With this criterion it appears that the 50 m sphere could be well resolved to 1.5 km depth with a 3 km bipole. Note that on the basis of signal strength the maximum depth of detection is almost 1.5 km for all values of L but for short bipoles the dynamic range limit is exceeded at much shallower depths. This is another way of stating that the best detectability is achieved as the bipole length increases and the incident fields become uniform with depth.

The only electric fields that can be assumed to be constant from the surface to depths on the order of 1-2 km are natural low frequency EM fields. These fields decay exponentially with

depth. The decay rate is the 'skin depth' δ given by Equation (4.12). The fields can be assumed to be approximately constant with depth when the skin depth is larger than the depth of interest. If δ was 4 km in a 10 Ohm-m half-space a uniform field to a depth of 2 km would be achieved with a frequency lower than 0.16 Hz. Unfortunately, the natural field spectrum has a pronounced low in the 0.3 to 5 Hz band but picks up again at 0.03 Hz. So for good signal levels a frequency of 0.03 Hz would be used yielding a skin depth of ~9 km – more than enough to provide a uniform field at up to 2 km. The ratio of the electric to magnetic field at the Earth's surface is given by $\frac{E}{B} = \sqrt{\frac{2\pi f \rho}{\mu_0}}$, where $\mu_0 = 4\pi \times 10^{-7}$. A typical value for the magnetic field at 0.03 Hz is about 10^{-10} Tesla (T) so the accompanying E-field over a 10 Ohm-m ground would be 1.2×10^{-7} V/m. Applying Equation (5.5) yields a value for the secondary field on the surface for a resistive sphere of radius 50 m at a depth of 1.0 km of ~ 1.5×10^{-11} V/m – a factor of only 15 above the anticipated noise level of a field receiver. Given that a useful E-field anomaly should be ten-times the noise level it does not seem feasible to monitor features of this size at depths of a kilometer or more using natural fields.

6. Advantages and Limitations of Electrical and EM Techniques in Detecting Resistors

6.1 Magnetometric resistivity (MMR)

For a horizontally layered medium there are no magnetic fields on the surface from the two current injection electrodes for a surface bipole transmitter, except for the fields arising from the wires on the surface connecting the electrodes to the power supply. Currents do flow in the half-space and perturbations of those currents caused by inhomogeneities give rise to magnetic fields

on the surface. The distortion caused by a resistive sphere is due to an induced opposing electric dipole located at the center of the sphere. This virtual dipole was used to calculate the anomalous electric fields at the surface when the sphere at depth was subjected to an incident electric field. This dipole is also a source for a magnetic field given by the simple form Biot and Savart's Law, Equation (4.6). At a point on the surface, a distance z directly above the sphere, the field **B** is in the y-direction, is negative and is given simply by:

$$B_Y = \frac{\mu_0 p}{4\pi z^2}, \tag{6.1}$$

where $p = IdL$ is the electric dipole moment.

p is given by: $$-\frac{E_{0X} 4\pi R^3}{2\rho_1}, \text{ when } \rho_2 \gg \rho_1 \tag{6.2}$$

so finally, B_Y is: $$B_Y = \frac{E_{0X}\mu_0}{2\rho_1}\frac{R^3}{z^2}, \tag{6.3}$$

and E_{0X} is given by Equation (5.6).

A plot of B_Y (in Teslas) as a function of the depth of a 50 m resistive sphere and L for a source $I\rho_1 = 1000$ is presented in Figure 17.

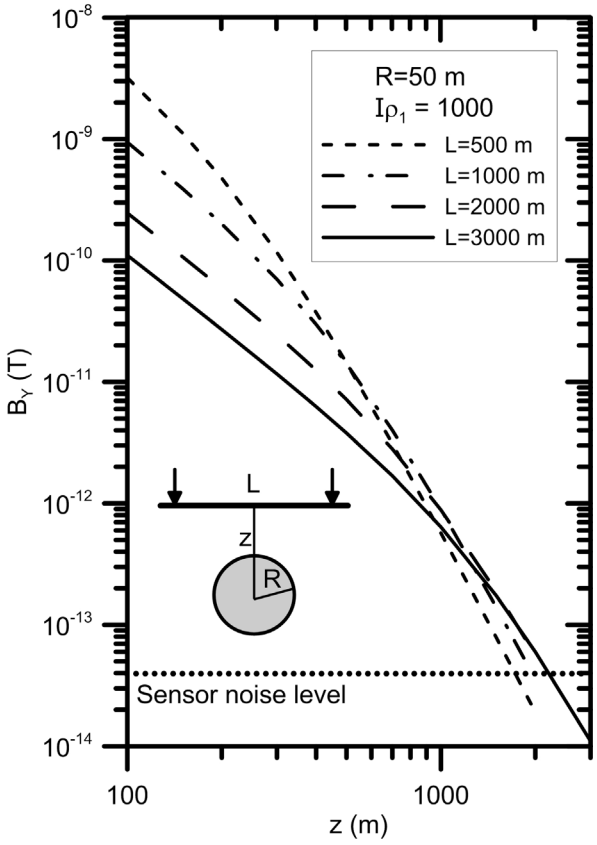

Figure 17. B_Y (in Teslas) as a function of the depth of a 50 m resistive sphere and for various L and a source $I\rho_1 = 1000$.

The noise level for a low frequency induction coil magnetometer (i.e., EMI BF-4 or Zonge ANT 4) is about 4×10^{-14} T at 0.5 Hz, and a typical value for the natural magnetic field at this frequency is about 10^{-12} T. Signals from a 50 m resistive sphere could apparently be well resolved to depths of 2 km. While this is comparable to the depth of detection using electric fields from large bipoles, note that this depth can be achieved with MMR with shorter bipoles. The other major advantage of MMR is that magnetic fields measured on the surface are much less affected by shallow inhomogeneities of the kind shown in Figure 14.

6.2 Magnetotellurics (MT)

The MT results for the model of a 50 m thick layer at a depth of 1.0 km show an anomaly of 2.3% for a 1000 Ohm-m layer resistivity and 18.5% for a 10 Ohm-m layer. The induced currents flow horizontally in a layered medium, so one may expect that they will have little sensitivity to thin resistive layers at depth. As with all resistivity and EM techniques, field results will be influenced by unavoidable lateral inhomogeneities in geology at the sounding location, which will affect the calculated apparent resistivity and mask the desired response from a deep layer or target. This is usually referred to as geologic noise. A layer response of 2.3% would not be discernable in a practical survey response.

6.3 EM Techniques Using Subsurface Sources

When EM sources are deployed at depth in the half-space the situation changes and certain sources induce vertical currents that are sensitive to the transverse, vertical, resistivity that in turn is sensitive to the presence of flat lying resistive bodies. Analysis of the response of magnetic and electric dipole sources in the conducting half-space shows that there are two fundamental modes of induction, one that induces fields in the horizontal plane, the TE mode, and one that induces fields in vertical planes, the TM mode. A vertical magnetic dipole, a horizontal loop, is a pure TE source that produces only horizontal currents whether on the surface or in the ground. A vertical electric dipole or bipole in the ground is a pure TM source that induces fields in vertical planes. A horizontal electric dipole or bipole and a horizontal magnetic dipole produce mixed TE and TM modes whether on the surface or at depth. If these sources are on the surface the boundary condition of no vertical current flow into the air forces the EM fields to flow only

horizontally, but in the half-space vertical currents can flow. Unlike the DC fields of electric bipoles or dipoles that are influenced by longitudinal resistivities the TM induced fields are responsive to the transverse resistivity.

The detection of flat lying resistive formations is a major objective of petroleum exploration. Several studies have shown that vertical and horizontal time varying electric dipoles and electric field receivers on the ocean bottom are remarkably sensitive to resistive layers beneath the ocean floor. The method is known as controlled source EM (CSEM) and the most common configuration uses a horizontal electric bipole source towed above the sea floor operating in the 0.1 to 1.0 Hz frequency range and with stationary electric and magnetic field sensors located on the ocean floor. Figure 18 shows an example of the response of a 100 Ohm-m layer 50 m thick at a depth of 1.0 km beneath the sea floor as a function of frequency and receiver offset. At the DC response, this layer has a peak response at about an offset of 2 km that is ~30% larger than the half-space without the layer. As the frequency increases, the peak response shifts to greater offsets and to higher frequencies, leading to a remarkable anomaly of over twice the half-space response at offsets between 6 and 10 km at a frequency of 0.03 Hz. Detailed analysis of the current flow patterns shows that around 0.03 Hz the currents at the depth of the layer, at an offset of 6 km, are vertical and that the introduction of the resistive layer causes a major change of current flow pattern that manifests itself as a big change in the horizontal field on the ocean floor. In an elegant analytical study of this effect, Cuevas and Alumbaugh [2011] show that far from the source the TM mode from the horizontal electric dipole diffuses in a waveguide-like fashion in the resistive layer, leaking field into the surrounding conductor and enhancing the field measured at large offsets.

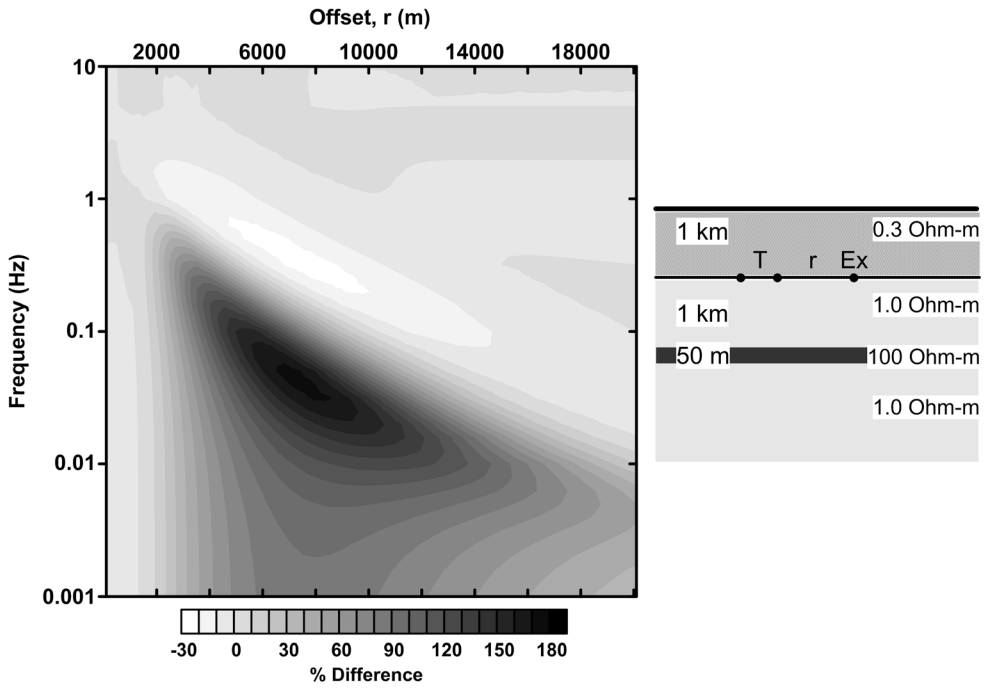

Figure 18. Response of a 100 Ohm-m layer 50 m thick at a depth of 1.0 km beneath the sea floor as a function of frequency and receiver offset.

On land, a vertical bipole provides the required TM mode and would be practical if an uncased well near the injection well were available. (A plastic or fiberglass cased well could also be used if equipped with a metallic section at the bottom connected by cable to the surface.) Cuevas and Alumbaugh [2011] modeled the response of a 100 Ohm-m resistive layer 250 m thick in a 1.0 Ohm-m background. A vertical dipole source and vertical electric receiver were placed 1.0 km above the layer separated horizontally by 250 m. The layer response was revealed most distinctly in the step function time domain response for the vertical component of the electric field. The time domain response shows a very pronounced anomaly from the layer, a decrease from the whole-space response of almost 80% at 10 seconds after source current shutoff. A simulation more representative of the 50 m resistive layer used in the previous models is shown in Figure 19. The vertical bipole source is located at a depth of 500 m and the horizontal electric field Ex is

calculated on the surface at an offset of 250 m. The resistive layer depresses the response by almost 40% at 100 ms into the transient. The DC response for this configuration is only a few percent. Streich et al. [2016] also showed a significant anomaly for a horizontal electric dipole for the resistor in a conductive half-space. In a separate study, Alumbaugh et al. [2010] showed that the vertical electric dipole - Ez receiver configuration retained good sensitivity when the layer was reduced to a finite width slab. This configuration shows great promise for detecting and monitoring the emplacement of tabular zones of resistive CO_2.

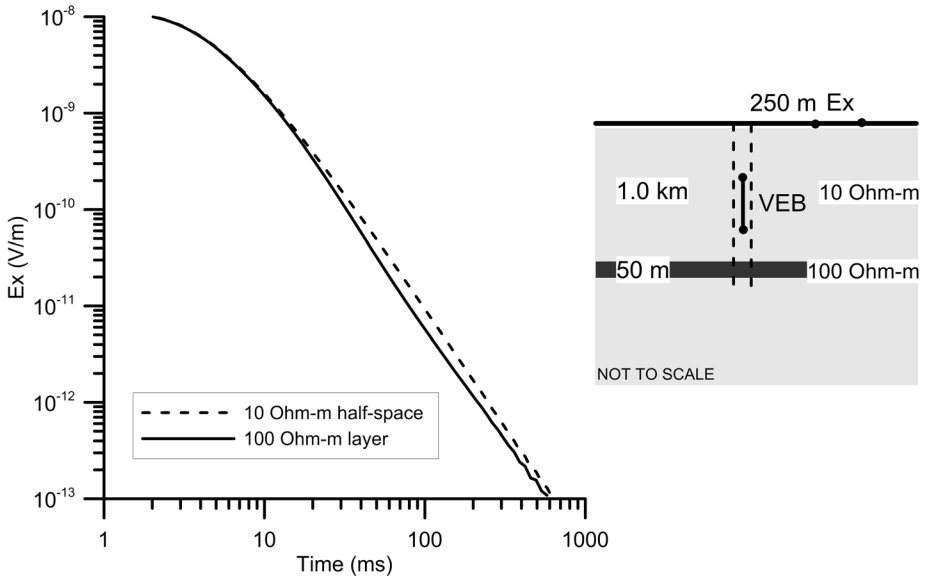

Figure 19. The time domain response of a 50-m thick layer of 100 Ohm-m in a 1.0 Ohm-m half-space using vertical electrical bipole (VEB) as a source and a surface horizontal E-field receiver (Ex).

6.4 Resistivity Techniques Using Borehole Sources

The resistive layer model can be used to illustrate the response for a current source in the ground. The horizontal electric field for a pole source on the surface and at a depth of 1.0 km over a 50 m

layer of 100 Ohm-m resistivity at 900 m is shown in Figure 20. The half-space resistivity is 10 Ohm-m. The fields are calculated for a current of 1.0 ampere.

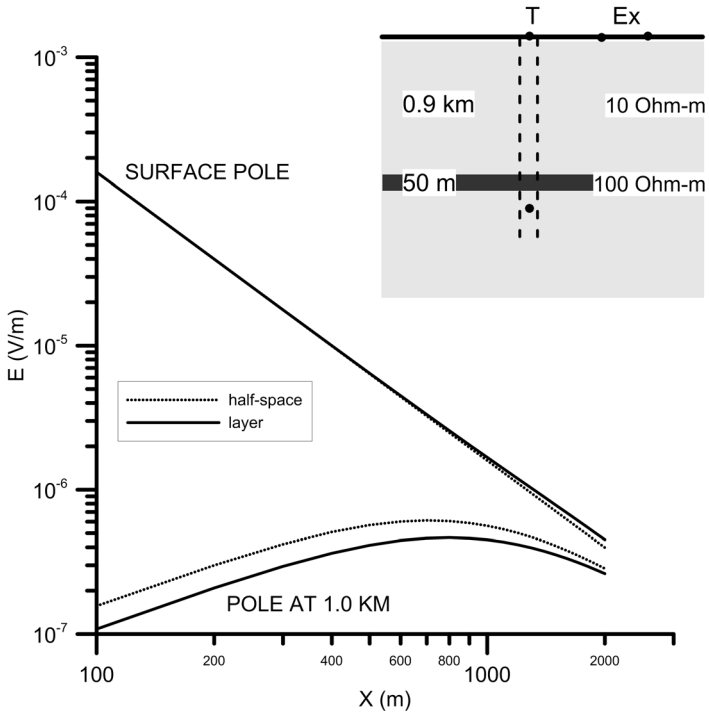

Figure 20. Electric field on the surface for a pole source on the surface and at depth with and without a resistive 50 m thick layer at 900 m depth.

For the surface pole, the resistive layer slightly increases the field beyond a kilometer: the field is increased by about 13% at 2 km. This is compatible with the responses observed for the large spacing Schlumberger soundings shown in Figure 10. For the subsurface pole, the response is of course much less because the source is far away. The layer shields the current and shifts the E-field response down over the range of E-field measurements. The decrease in field caused by the layer at small offsets is ~30%, much larger than the anomaly seen from the surface pole. When current electrodes of opposite polarity are energized at the surface and a depth of 1.0 km,

creating a vertical bipole the layer response is 66% above the half-space response. It appears that the sensitivity to a resistive layer improves for surveys incorporating current sources below the layer. The increase in layer sensitivity might justify the field costs of implanting a subsurface electrode.

Borehole-to-surface electrical surveys could be conducted using the casing itself as an element of the survey configuration. One configuration involves injecting current directly into the casing at the surface, with the return current connected through a long wire on the surface. Another configuration consists of a current source (pole) at the bottom of the casing, with the return source located a long distance away on the surface. In both cases, it is expected that current will be carried down or up the casing with diminishing amplitude as current leaks radially off the casing into the surrounding formations. In principle, the effect is supposed to inject more current in the vicinity of the target and thus to create a bigger distortion, or anomaly, in the electric field measured on the surface.

The first quantitative analyses for fields arising in the ground from current sources in a metal casing were presented by Kaufman [1990], Vail [1989], and Schenkel and Morrison [1990, 1994]. Recent developments in this area are described by Puzyrev et al. [2017] and references therein.

The idea of using the casing as a source is to redistribute the current from a point source to the current leaving a vertical line (casing) source. Because the casing has a finite conductivity there is a balance achieved between current flowing down the casing and current leaking radially off the casing. Schenkel and Morrison [1990] found that the falloff of the radial current, and the casing current, was exponential of the form $e^{-z/\sqrt{\rho_f S_c}}$, where z is the depth, ρ_f is the formation resistivity, and S_c is a kind of casing conductance given by $S_c = \pi D t \sigma_c$, where D, t, and σ_c are the diameter, thickness, and conductivity, respectively, of the casing. Schenkel and Morrison [1990] called the depth at which $z = \sqrt{\rho_f S_c}$ the conduction length – the depth at which the current leaving the casing has fallen to 1/e its value at the surface. In other words, ~63% of the current has leaked into the formation by the conduction depth. One should not expect the casing to add much radial current to the half-space beyond two conduction depths, up to which 86% of the current has leaked radially off the casing.

The conduction length, for typical casings, in low resistivity sediments is on the order of only 200-400 m. If the casing is on the order of 2 km long and depths of investigation of greater than 1.0 km are desired, the casing distributes the current over a relatively short distance and it will look similar to a point source at the surface. Having the casing poses no significant advantage in getting current down to the region of interest. If the formation resistivity were to be 100 Ohm-m, say in a thick carbonate sequence, the conduction length increases to ~1.5 km and enhanced anomalies might be expected from target zones at depths of this order.

The simplest model for testing the sensitivity of casing sources is the thin resistive layer in a uniform half-space shown in Figure 20. The dashed vertical lines indicate the casing. Current electrodes can be located at the surface on the casing, at depth in the casing or at the top and bottom creating a kind of vertical bipole. As for the model without the casing, the horizontal electric field is plotted versus distance from the borehole. The fields are calculated with and without the layer to show how the casing influences the detection of the layer. The anomaly, the percent difference in response introduced by the layer is defined by:

$$\%Difference = \frac{E_{half-space} - E_{with\,layer}}{E_{half-space}} \cdot 100 \ [\%]$$

So if the layer diminishes the field seen on the surface the percent difference is positive, and it is negative if the layer increases the field on the surface. In this analysis, steel casing with a resistivity of 10^{-6} Ohm-m, a diameter of 0.228 m (O.D. ~9.0 in), and a wall thickness of 0.127 m (0.5 in) was used. The conduction depth in the 10 Ohm-m half-space is ~420 m. An analysis of the effects of placing the source at the top or bottom or as a vertical bipole is summarized in Table 3.

	Pole at surface	**Pole at 1.0 km**	**1.0 km vertical bipole**
No casing	-13%	30%	-66%
Casing	-13%	-10%	-49%

Table 3. Percentage change from half-space response caused by 50-m thick layer of 100 Ohm-m at a depth of 900 m, with and without casing (model of Figure 20).

As discussed above, the casing distributes the current over a relatively short distance and the response is identical to that of a point source at the surface. Having the casing poses no

significant advantage in getting current down to the region of interest. Placing the pole at the bottom of the casing, below the layer yields a rather modest layer anomaly of only 10%, or *1/3 the anomaly created by the same pole in the absence of casing.* By distributing the radial current flow up the casing the shielding effect of the resistive layer on a point source below the layer is diminished. The current leaving the casing becomes uniform on the scale of the layer and consequently the response becomes the usual weak response of a resistive layer in a longitudinal field. Interestingly, this effect is muted for the vertical bipole source. The layer anomaly drops from 66% to 49% upon the introduction of casing. It appears that the casing, energized as a vertical bipole, is an excellent source for detecting and monitoring a resistive layer at depths comparable to the casing depth.

7. Monitoring of shallow CO_2 leaks

Monitoring outside of the reservoir is mostly important for leakage detection and serves regulatory as well as public perception purposes. Although unlikely, the increased reservoir pressure can lead to leakage of reservoir brine (high salinity water) or CO_2 into shallow aquifers [Birkholzer et al., 2009]. Reservoir brine is mostly of high salinity and can therefore increase salinity levels in groundwater above acceptable drinking water limits. At the same time, leaked brine is characterized by a strong decrease in electrical resistivity, caused by the dissolved salt. Only a few studies [e.g., Strazisar et al., 2009; Lamert et al., 2012; Dafflon et al., 2013; Trainor-Guitton et al., 2013; Auken et al., 2014] have investigated the electrical signature of dissolved CO_2 in groundwater. Both Lamert et al. [2012] and Dafflon et al. [2013] find that electrical resistivity initially decreases after the CO_2 injection, owing to an increase in bicarbonate and dissolved species. Dafflon et al. [2013] also find that as pH decreases further, resistivity

rebounds toward initial conditions, due to a reduction of dissociated species. These challenges are critical for detecting dissolved CO_2 in potable aquifers. Electrical monitoring would have to consider fluid salinity and the complex geochemical reactions of CO_2 with these fluids, since the resulting anomalies could be both resisitive and conductive.

8. References

Alumbaugh, D., N. H Cuevas, J. Chen, G. Gao, and Brady, J. (2010), Comparison of sensitivity and resolution with two marine CSEM exploration methods, Soc. of Explor. Geophysicists Expanded Abstracts, 3893–3897.

ANT-4 Magnetic field sensor, Zonge International, http://zonge.us/wp-content/uploads/2013/06/SPEC_Ant-5643.pdf, accessed 12.03.2015.

Archie, G. (1942), The electrical resistivity log as an aid in determining some reservoir characteristics, Trans., AIME 146, 54–62.

Auken, E., J. Doetsch, G. Fiandaca, A. V. Christiansen, A. Gazoty, A. G. Cahill, and R. Jakobsen (2014), Imaging subsurface migration of dissolved CO2 in a shallow aquifer using 3D time lapse electrical resistivity tomography, Journal o. Applied Geophysics, 101, 31–41.

Barker, R. D. (1989) Depth of investigation of collinear symmetrical four-electrode arrays, Geophysics, 54, 1031–1037.

BF-4 Magnetic Field Induction Sensor, Schlumberger, https://www.slb.com/~/media/Files/rd/technology/product_sheets/emi_bf_4.pdf, accessed 12.03.2015.

Birkholzer, J. T., Q. Zhou, and C.-F. Tsang (2009), Large-scale impact of CO2 storage in deep saline aquifers: a sensitivity study on pressure response in stratified systems, Int. J. Greenh. Gas Control, 3, 181–194.

Cuevas, N.H. and D. Alumbaugh, (2011) Near-source response of a resistive layer to a vertical or horizontal electric dipole excitation, Geophysics, 76, F353–371.

Dafflon, B., Y. Wu, S. S. Hubbard, J. T. Birkholzer, T. M. Daley, J. D. Pugh, J. E. Peterson, and R. C. Trautz (2013), Monitoring CO2 intrusion and associated geochemical transformations in a shallow groundwater system using complex electrical methods: Environmental Science and Technology, 47, 314–321, doi: 10.1021/es301260e.

Edwards, R. N., and M. N. Nabighian (1991), The Magnetometric resistivity method, Investigations in Geophysics 3, Vol. 2., Soc. of Explor. Geophysicists, Tulsa.

Gueguen, Y. (1994), Introduction to the physics of rocks, Princeton.

http://appliedgeophysics.berkeley.edu

Kamel, M. H., W. M. Mabrouk, and A. I. Bayoumi (2002), Porosity estimation using a combination of Wyllie-Clemenceau equation in clean sand formation from acoustic logs, Journal of Petroleum Science Engineering, 33, 241–251. doi: 10.1016/S0920-4105(01)00169-3

Kaufman, A. (1990), The electrical field in a borehole with casing, Geophysics, 55, 29–38.

Keller, G.V. (1966), Electrical properties of rocks and minerals, in Handbook of physical constants, revised ed.: S. P. Clark, Jr., Ed., New York, GSA Memoir 97.

Keller, G.V. (1987), Rock and mineral properties, in Nabighian, M.N., Electromagnetic Methods in Applied Geophysics, Vol. 1, Theory, Soc. of Explor. Geophysicists, Tulsa.

Kennedy, W. D., and D. C. Herrick (2012), Conductivity models for Archie rocks, Geophysics, 77, WA109–WA128.

Lamert, H., H. Geistlinger, U. Werban, C. Schütze, A. Peter, G. Hornbruch, A. Schulz, M. Pohlert, S. Kalia, M. Beyer, J. Grosmann, A. Dahmke, and P. Dietrich (2012), Feasibility of geoelectrical monitoring and multiphase modeling for process understanding of gaseous CO_2 injection into a shallow aquifer, Environ. Earth Sci., 67, 447–462.

Mabrouk, W. M., K. S. Soliman, and M. A. Tawfic (2012), An enhancement of the formation factor parameters a and m, Exploration Geophysics, 87–94.

Nakatsuka, Y., Z. Xue, H. Garcia, and T. Matsuoka (2010), Experimental study on CO2 monitoring and quantification of stored CO2 in saline formations using resistivity measurements. International Journal of Greenhouse Gas Control, 4, 209–216.

Parker, R. L. (1977), Understanding inverse theory, Ann. Rev. Earth. Planet. Sci., 5, 35–64.

Puzyrev, V., E. Vilamajo, P. Queralt, J. Ledo, and A. Marcuello (2017), Three-dimensional modeling of the casing effect in onshore controlled-source electromagnetic surveys: Surveys in Geophysics, 38, 527–545.

Schenkel, C. J. and H. F. Morrison (1990), Effects of well casing on potential field measurements using downhole current sources, Geophysical Prospecting, 38, 663–686.

Schenkel, C. J. and H. F. Morrison (1994), Electrical resistivity measurement through metal casing, Geophysics, 59, 1072–1082.

Schlumberger (1989), Log Interpretation Principles/Applications, Schlumberger Educational Services, Houston, TX.

Streich, R. (2016), Controlled-Source Electromagnetic Approaches for Hydrocarbon Exploration and Monitoring on Land. Surveys in Geophysics, 37, 47-80.

Telford, W. M., L. P. Geldart, and R. F. Sheriff (1990), Applied geophysics, Cambridge University Press.

Trainor-Guitton, W. J., A. Ramirez, X. Yang, K. Mansoor, Y. Sun, and S. Carroll (2013), Value of information methodology for assessing the ability of electrical resistivity to detect CO_2/brine leakage into a shallow aquifer, Int. J. Greenhouse Gas Control, 18, 101–113.

Vail, W.B. (1989), Method and apparatus for measurement of electronic properties of geological formations through borehole casing: U.S, patent 4,882,542.

Vozoff, K. (1991), The magnetotellurics method, Investigations in Geophysics 3, Vol. 2., Soc. of Explor. Geophysicists, Tulsa.

Ward, S.H. (1967), Electromagnetic theory for geophysical applications, Mining Geophysics, Vol. 2, Soc. of Explor. Geophysicists, Tulsa.

Ward, S. H., and G. W. Hohmann (1987), Electromagnetic theory for geophysical applications, in Electromagnetic methods in applied geophysics, Investigations in Geophysics 3, Vol. 1., Soc. of Explor. Geophysicists, Tulsa.

Waxman, M. H., and L. J. M. Smits (1968), Electrical conductivities in oil-bearing shaly sands: Society of Petroleum Engineering Journal, June 1968, p. 107-122.

9. Acronyms

B	Magnetic field
CSEM	Controlled Source ElectroMagnetic
CO_2	Carbon Dioxide
DC	Direct Current
E	Electric field
EM	Electromagnetic
ERT	Electrical Resistance Tomography
H	Magnetic Field ($B = \mu H$)
MMR	MagnetoMetric Resistivity
MT	Magnetotellurics
TDS	Total Dissolved Solids